Identification of anti-Parkinson's Disease Lead Compounds from *Aspergillus ochraceus* Targeting Adenosin Receptors A_{2A}

Linzhen Hu[+],*[a] Shuying Tian[+],[a] Rongrong Wu,[a] Zhou Tong,[a] Wen Jiang,[a] Ping Hu,[a] Xueyang Xiao,[a] Xueke Zhang,[a] Hui Zhou,[a] Qingyi Tong,[b] Yuanyuan Lu,[d] Zhiyong Huang,*[a, c] Yong Chen,[a] and Yonghui Zhang*[b]

Two novel alkaloids compounds together with fifteen know metabolites were identified from *Aspergillus ochraceus.* The stereochemistry features of the new molecules were determined via HRESIMS, NMR, ECD, and XRD analyses. Amongst these, compounds two compounds exhibited potential efficacy as anti-Parkinson's disease with the EC_{50} values of 2.30 and 2.45 μM, respectively. ADMET prediction showed that these compounds owned favorable drug-like characteristics and safe toxicity scores towards CNS drugs. Virtual screening analyses manifested that the compounds exhibited not only robust and reliable interactions to adenosine receptors A_{2A}, but also higher binding selectivity to A_{2A} receptors than to A_1 and A_3 receptors. Molecular dynamics simulation demonstrated the reliability of molecular docking results and the stability of the complexes obtained with the novel compounds and A_{2A} receptors in natural environments. It is the first time that anti-PD lead compounds have been identified from *Aspergillus ochraceus* and targeting adenosine A_{2A} receptors.

1. Introduction

Parkinson's disease (PD) is a typical neurodegenerative disease. The main pathological characteristics of PD are the selective loss of dopaminergic neurons (DA) in the substantia nigra and the chronic accumulation of α-synaptic nuclear proteins forming Lewy bodies.[1] The clinical medications comprise mainly dopaminergic agents and non-dopaminergic drugs. However, the former, such as levodopa, carbidopa, rasagiline, etc., lacked long-term efficacy as well as being limited by adverse effects of the motor syndrome like "wearing-off", oscillation, and dyskinesia.[2] The emerging non-dopaminergic agents, adenosine receptor type 2 A ($A_{2A}R$) antagonists, via the blockade of $A_{2A}R$ in striatopallidal neurons, appeared to possess prospective effectiveness on the control of the neurodegenerative processes of PD.[3] Nevertheless, few drugs were approved as A_{2A} antagonists targeting $A_{2A}R$ for PD treatment. Thus, sincere efforts to discover more lead molecules of $A_{2A}R$ antagonists for PD administration are urgently needed.

Aspergillus ochraceus (Aspergillaceae), a filamentous fungus, has been extensively investigated in recent decades for its secondary metabolites and related bioactivities. *A. ochraceus* contains a plethora of diverse secondary metabolites such as ochratoxins,[4] sesquiterpenoids,[5] pyrones,[6] lactones,[7] steroids,[8] and alkaloids,[9] while most of these metabolites have presented promising biological effects of antiinsectan,[10] antibacterial,[9d] anti-inflammatories,[11] antiviruses,[9c] antitumors,[6] and neuroprotective.[12] Herein, seventeen diverse metabolites including a new benzodiazepine alkaloid, namely circumdatin N (**7**), and a new oxazole derivative, namely ochracesol A (**17**), were discovered from *A. ochraceus* (Figure 1). The stereochemistry characteristics of new molecules were determined via extensive spectra methods, TD-DFT quantum-chemical prediction on ECD, and X-ray diffraction analyses. Amongst these isolates, compounds **14** and **15** exhibited promising protected effectiveness towards MPP^+-induced SH-SY5Y cells with the EC_{50} values of 2.30 and 2.45 μM, respectively. ADMET prediction by Discovery Studio 2020 (DS20) presented that **14** and **15** have good drug-like characteristics of fitting Lipinski's rules, CNS drugs features, and safe

[a] *Prof. L. Hu,[+] S. Tian,[+] R. Wu, Z. Tong, W. Jiang, P. Hu, X. Xiao, X. Zhang, H. Zhou, Prof. Z. Huang, Prof. Y. Chen*
Hubei Collaborative Innovation Centre for Green Transformation of Bio-Resources
School of Life Sciences
Hubei University
430062 Wuhan (China)
E-mail: linzhenhu@hubu.edu.cn
[b] *Prof. Q. Tong, Prof. Y. Zhang*
School of Pharmacy, Tongji Medical College
Huazhong University of Science and Technology
430030 Wuhan (China)
E-mail: zhangyh@mails.tjmu.edu.cn
[c] *Prof. Z. Huang*
Tianjin Institute of Industrial Biotechnology
Chinese Academy of Sciences
300308 Tianjin (China)
E-mail: huang_zy@tib.cas.cn
[d] *Dr. Y. Lu*
Maternal and Child Health Hospital of Hubei Province
Tongji Medical College
Huazhong University of Science and Technology
430070 Wuhan (China)
[+] *These authors contributed equally to this work.*

Supporting information for this article is available on the WWW under https://doi.org/10.1002/open.202100022

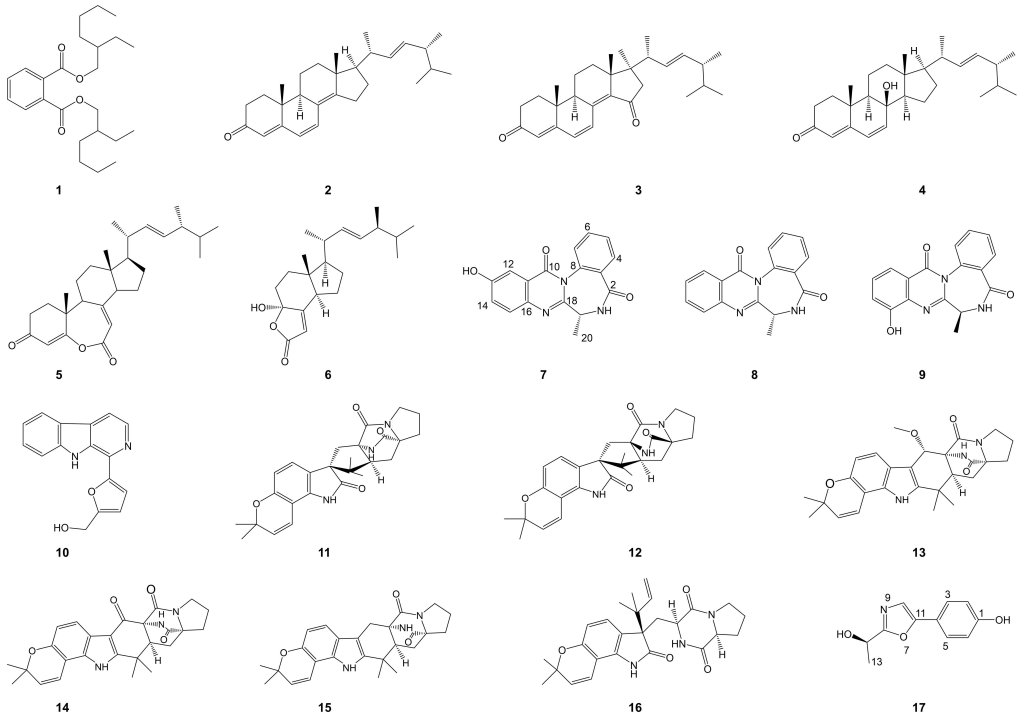

Figure 1. Structures of compounds **1**–**17** from *Aspergillus ochraceus*.

scores of toxicities. Virtual screening studies via LibDock and CDOCKER modules in DS20 showed that **14** has a higher dock score and approaching interaction energy compared to istradefylline, an approved $A_{2A}R$ antagonist in Japan. AutoDock 4.2.6 with MGLTools 1.5.6 (ADT) analyses manifested that **14** exhibited robust and reliable interaction with $A_{2A}R$ (PDB code, 3EML) along with the highest binding affinities of −10.27 kcal/mol, and the lowest inhibition constants of 29.61 nM, respectively. ADT also predicted that **14** presented higher binding affinity to $A_{2A}R$ than to A_1R (PDB code, 5N2S) and A_3R (PDB code, 1OEA). Besides, Molecular dynamics simulation demonstrated the reliability of molecular docking results and the stability of **14**-$A_{2A}R$ complex in natural environments. These results provided us the first insight into that **14** could serve as a promising lead compound of targeting $A_{2A}R$ for exploring anti-PD drugs.

A modified PDA medium contained CYP450 oxidase inhibitor 8-geranyloxypsoralen was utilized for *A. ochraceus* culture. An ethanol extract from the whole rice fermentation of *A. ochraceus* was experienced extensive chromatographic methods to afford one new benzodiazepine alkaloid circumdatin N (**7**), and one new oxazole derivative ochracesol A (**17**), together with fifteen known isolates (**1**–**6** and **8**–**16**). According to the analyses of the NMR data with those reported in the literatures, these known compounds were confirmed as di-(2-ethylhexyl) phthalate (**1**),[13] ergosta-4,6,8(14),22-tetraen-3-one (**2**),[14] gymnasterone D (**3**),[15] isocyathisterol (**4**),[16] herbarulide (**5**),[17] demethylincisterol A2 (**6**),[18] (+)-circumdatin F (**8**),[19] circumdatin G (**9**),[19] perlolyrine(**10**),[20] notoamide B (**11**),[21] versicolamide B (**12**),[22] notoamide F (**13**),[23] notoamide I (**14**),[24] stephacidin A (**15**),[21] and notoamide C (**16**).[21]

2. Results and Discussion

2.1. Structural Elucidation of the Secondary Metabolites

Compound **7** (circumdatin N), as the thirteenth new benzodiazepine derivative,[9h] was deduced the molecular formula $C_{17}H_{13}N_3O_3$ by the HRESIMS pseudo molecular ion peak at *m/z* 330.0839 $[M+Na]^+$ (calcd for $C_{17}H_{13}N_3NaO_3$, 330.0855), demanding thirteen degrees of unsaturation. The IR spectroscopic analysis implied the molecule with the characteristic groups for hydroxyl (3375 cm^{-1}), carbonyl (1680 cm^{-1}), and aromatic rings (1614 cm^{-1} and 1537 cm^{-1}). Owing to the data of the ^1H and ^{13}C NMR (Table 1), together with the HSQC spectrum (see Figures S1–S6 in the Supporting information), this metabolite was characterized the presence of one methyl (δ_C14.9; δ_H 1.50 d, J= 6.5 Hz), one methine (δ_C 49.3; δ_H 4.21 p, J=12.5, 6.5 Hz), seven olefinic/unsaturated carbons with protons (δ_C 109.8, 124.6, 128.6, 128.7, 128.8, 129.0, and 130.6; δ_H 7.44 d, J=2.8 Hz; 7.31, dd, J=8.8, 2.8 Hz; 7.58, br s; 7.55, m; 7.76, dd, J=7.6, 1.5 Hz; 7.60, br s; 7.64, m), and eight proton-free olefinic/unsaturated carbons (δ_C 122.0, 131.4, 133.3, 138.5, 153.1, 157.7, 160.9, and 166.8). These characteristics were very similar to those of (+)-circumdatin F (**8**)[19] and circumdatin G,[19] whilst the only differentiation between **7** and **8** was the additional presence of one hydroxyl substituted at C-13 of the benzene ring (δ_C 157.7) in **7**, which fit the HRESIMS data analyses. The HMBC spectrum correlations (Figure 2) from H-12 to C-10, H-14 to C-12/C-16, H-15 to C-11, H-5 to C-3, H-6 to C-8, H-19 to C-18/C-2, Me-20 to C-18/C-19, and from NH (δ_H 8.74) to C-3/C-19/C-20 as well as the ^1H–^1H COSY spin systems of H-4/H-5/H-6/H-7 and H-14/H-15 confirmed the planar structure of **7** as a benzodiazepine

Table 1. ^{1}H NMR (400 MHz) and ^{13}C (100 MHz) Data for compounds **7** and **17** (δ in ppm, J in Hz).

No.	**7**[a]		**17**[b]	
	δ_H	δ_C	δ_H	δ_C
1				159.6
2		166.8	6.84 m	116.9
3		131.4	7.52 m	127.1
4	7.76 dd (7.6, 1.5)	128.8		120.7
5	7.55 m	128.7	7.55 m	127.1
6	7.64 m	130.6	6.86 m	116.9
7	7.60 br s	129.0		
8		133.3		166.4
10		160.9	7.21 s	120.1
11		122.0		153.7
12	7.44 d (2.8)	109.8	4.92 dd (13.4, 6.7)	64.3
13		157.7	1.59 d (6.7)	21.5
14	7.31 dd (8.8, 2.8)	124.6		
15	7.58 br s	128.6		
16		138.5		
18		153.1		
19	4.28 p (12.5, 6.5)	49.3		
20	1.50 d (6.7)	14.9		

[a] Record in DMSO-d_6. [b] Record in CH_3OH-d_4.

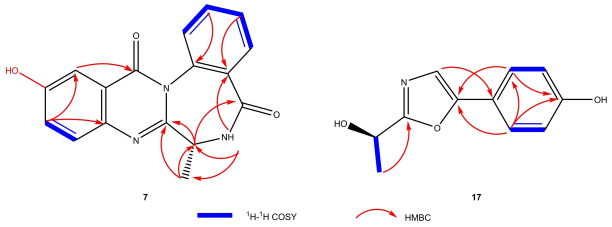

Figure 2. Key 2D NMR correlations of compounds **7** and **17**.

derivative, which was potentially biosynthesized via anthranilic acids and one alanine amino acid.[9h]

To tackle the stereoscopic configuration of C-19 in compound **7**, the electric circular dichroism (ECD) Cotton effects (CEs) were calculated using the time-dependent density functional theory (TD-DFT) methods. Gaussian 16 program was executed at the M06-2X-SCRF/def2-TZVP//M06-2X-SCRF/6-311G (d,p) level to collect the ECD spectra of 19*R*-**7**/19*S*-**7**. The calculated CEs of stereoisomer 19*R*-**7** exhibited good accordance with the experimental ones (Figure 3). Furthermore, the colorless crystals of **7** were eventually obtained, whose X-ray diffraction crystallographic analyses with Cu Kα radiation facilitated us to unambiguously testify its absolute stereochemistry as 19*R* (Figure 4, Flack parameter 0.06(6), CCDC 1961586).

HRESIMS analyses of compound **17** (ochracesol A) exhibited a hydrogen adduct cation at *m/z* 206.0724 $[M+H]^+$ (calcd for $C_{11}H_{12}NO_3$, 206.0817), matched with a molecular formula of $C_{11}H_{11}NO_3$ with the seven hydrogen deficiencies. The IR spectrum data showed its characteristic absorption bands of a hydroxyl group (3401 cm^{-1}) and an aromatic ring (1619 and 1504 cm^{-1}). The resonances of ^{1}H and ^{13}C NMR (Table 1), and HSQC correlations (see Figures S9–S14 in the Supporting information) allocated eleven carbons including six aromatic carbons (δ_C 116.9, 116.9, 127.1, 127.1, 120.7, and 159.6; δ_H

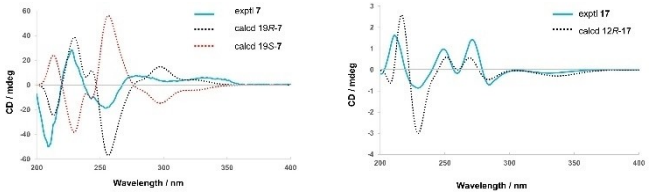

Figure 3. Experimental ECD spectra of **7** and **17**, and calculated ECD spectra of 19*R*-**7**, 19*S*-**7**, and 12*R*-**17**.

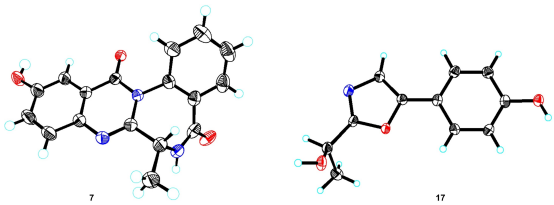

Figure 4. X-ray ORTEP drawing of **7** and **17**.

6.84 m, 6.89 m, 7.52 m, and 7.55 m) with one hydroxyl substitution, three olefinic/unsaturated carbons (δ_C 120.1, 153.7, and 166.4; δ_H 7.21 s), one oxygenated secondary carbon (δ_C 64.3; δ_H 4.92, dd, J = 13.4, 6.7 Hz), and one methyl (δ_C 21.5; δ_H 1.59, d, J = 6.7 Hz). Considering proton-free olefinic/unsaturated carbons (δ_C 153.7 and 166.4) with the larger chemical shifts, and combining the HRESIMS data analyses, we speculated that compound **17** should contain an oxazole ring, which also made the molecule to satisfy the preceding mentioned indices of the hydrogen deficiencies. Aside from the HSQC correlation signals, the planar skeleton of **17** was further characterized by 2D correlations of the HMBC and ^{1}H-^{1}H COSY spectra (Figure 2). Besides the HMBC correlations from H-3 to C-1 and H-5 to C-1/C-3, the presence of ^{1}H-^{1}H COSY cross-peaks of H-2/H-3 and H-5/H-6, together with their coupling constants approved the motif of para-disubstituted benzene. The 1-hydroxyethyl group was supported by the HMBC correlation signal of Me-13/C-12 along with the ^{1}H–^{1}H COSY spin system of H-12/H-13, which was assigned at C-8 of the oxazole ring by the presence of the HMBC correlations from Me-13/H-12 to C-8. Finally, the pivotal HMBC signal of H-3/C-11, H-5/C-11, and H-10/C-4 revealed the location of the oxazole ring at C-4 of the aromatic ring.

The above methods for the calculated ECD spectrum were also performed to confirm the absolute asymmetric center of **17**. The calculated ECD curve of 12*R*-**17** presented a good match with the experimental one (Figure 3). Fortunately, yielding high-quality colorless crystals via recrystallization, **17** followed the single-crystal X-ray diffraction analysis by Cu Kα radiation to be verified as 12*R* stereochemistry (Figure 4, Flack parameter 0.02(4), CCDC 1961585).

2.2. Biological Activities

1-methyl-4-phenylpyridinium (MPP^+), a parkinsonian neurotoxin metabolized after a systemic administration of 1-methyl-4-phenyl-1,2,3,6-tetrahydropyridine (MPTP), has been utilized as

an inducer towards SH-SY5Y cells for the study of the neuroprotective agents in PD.[25] Herein, along with levodopa as a positive control, the MTT assay was carried out to evaluate the anti-PD efficacy of all isolates through the PD model in vitro of MPP^+-induced SH-SY5Y cells, as previously described.[26] Intriguingly, most alkaloids generally showed potential neuroprotective effects to the MPP^+ insult SH-SY5Y cells whereas other classes of compounds did not (Table 2). Amongst these alkaloids, compounds **14** and **15** exhibited dose-dependent potency with the EC_{50} values of 2.30 and 2.45 μM, respectively (Table 2 and Figure 5).

Table 2. Anti-PD Activities of compounds **1**–**17** on SH-SY5Y cells and MPP^+-induced SH-SY5Y cells (μM).

Compounds	CC_{50}[a]	EC_{50}[b]	SI[c] (CC_{50}/EC_{50})
1	152.70	80.21	1.90
2	82.15	35.71	2.30
3	99.54	38.75	2.57
4	67.57	46.18	1.46
5	75.21	37.67	2.00
6	70.17	49.53	1.42
7	80.45	10.77	7.47
8	56.61	5.44	10.41
9	57.35	7.39	7.76
10	45.59	9.97	4.57
11	39.21	5.31	7.38
12	49.55	6.01	8.24
13	30.45	2.98	10.22
14	81.93	2.30	35.62
15	83.68	2.45	34.16
16	46.37	7.39	6.27
17	103.05	17.84	5.77
Levodopa (LD)	154.9	2.06	75.19

[a] 50% cytotoxic concentration value. [b] 50% effective concentration value. [c] Selectivity Index.

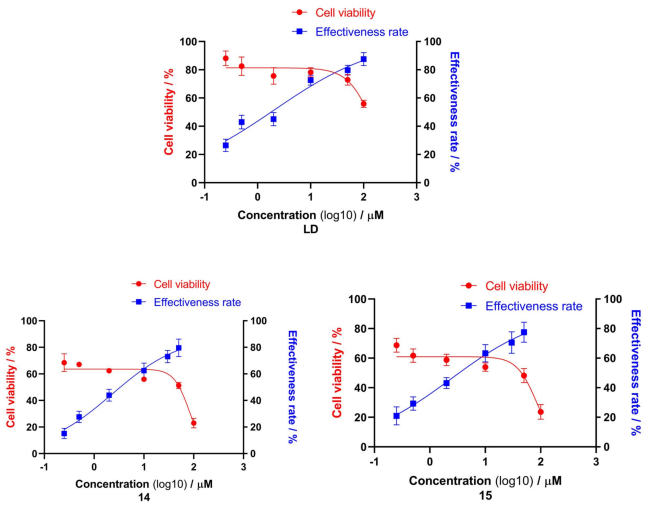

Figure 5. Effects on SH-SY5Y cells and MPP^+ insult SH-SY5Y cells viabilities of compounds **14** and **15** were evaluated using Levodopa (LD) as a positive control in vitro. Both values of CC_{50} and EC_{50} were calculated as mean values with standard deviations (n = 3, $P < 0.05$).

2.3. ADMET Prediction

All alkaloids were predicted for the absorption, distribution, metabolism, and excretion in the ADME Descriptors module of DS20, covering molecular weight (MW), octanol/water partition coefficient (AlogP), octanol/water distribution coefficient (logD), hydrogen bond donors (HBD), polar surface area (PSA), rotatable bonds, aqueous solubility level, blood-brain barrier level (BBB Level), and human intestinal absorption level (Absorption Level) properties (Table 3). The predicted ADME properties of compounds **14** and **15** featured drug-like characteristics as fitting Lipinski's rule of five states[27] and possessing appropriate profiles for CNS medicines.[28] Furthermore, safe and toxicity features were also considered in this research, and **14** and **15** displayed no Ames mutagenicity, less developmental toxicity potential, and relative safe data on rodent carcinogenicity (Table 4). These predictions imply that **14** and **15** are preferable safety, and they can be regarded as probable leading compounds.

2.4. Receptor-Based Virtual Screening

Adenosine receptors (ARs), as the G protein-coupled receptors, have several subtypes such as A_1, A_{2A}, and A_3, and in which A_{2A} exits in the basal ganglia with high density and plays a pivotal role in the regulation of motor movements. It was reported that highly selective A_{2A} antagonists could enhance the locomotor activity, reinforce the effects of levodopa, and attenuate the progress of dyskinesia by blocking $A_{2A}R$.[29] Molecules with core motifs such as piperazine, pyrimidine/pyridine, or oxazole structures have been utilized as $A_{2A}R$ antagonists for PD therapy exits in the basal ganglia with high density and play a pivotal role in the regulation of motor movements.[29] Considering the encouraging activity on MPP^+-induced SH-SY5Y cells and the analogous motifs of most alkaloids, virtual screening studies via LibDock and CDOCKER modules in DS20 were performed to predict hit compounds. The results exhibited that **14** has a higher dock score and an approaching CDOCKER interaction energy compared to istradefylline, an approved $A_{2A}R$ antagonist in Japan (Table 5). ADT programme was carried out for virtual screening via molecular docking. Autodock uses grid boxes for the definition of the binding sites. For 3EML, the grid size was designated at 90×90×90 (x, y, and z) points, with the grid box centered at x, y, and z dimensions of −5.237, −6.854, and 54.678, respectively. 5N2S, the grid size: 90×90×110 (x, y, and z) points, the grid center: 102.1×126.4×30.4 (x, y, and z) dimensions; 1OEA: the grid size: 90×100×90 (x, y, and z) points, the grid center: −8.441×−9.492×−1.95 (x, y, and z) dimensions. All above receptors were set with the grid spacing at 0.375 Å. The ligand molecule with the highest negative binding energy was considered to have the best binding affinity to the receptor.[30] The data analyses manifested that **14** exhibited robust and reliable interaction with $A_{2A}R$ (PDB code, 3EML) along with the highest binding affinity of −10.27 kcal/mol, and the lowest inhibition constant of 29.61 nM, respectively (Table 5). Based upon the results, further insight into the

Table 3. Prediction for the adsorption, distribution, metabolism, and excretion properties of compounds **7**–**17**.

Compounds	MW[a]	AlogP[b]	logD[c]	HBD[d]	PSA[e]	Rotatable Bonds[f]	Solubility Level[g]	BBB Level[h]	Absorption Level[i]
7	307.3	1.75	1.75	2	82	0	3	3	0
8	291.3	1.99	1.99	1	61.77	0	2	3	0
9	307.3	1.75	1.75	2	82	0	3	3	0
10	264.3	2.99	3.21	2	62.05	2	2	2	0
11	447.5	1.47	1.47	2	87.74	0	2	3	0
12	447.5	1.47	1.47	2	87.74	0	2	3	0
13	461.2	2.62	2.62	2	83.66	1	2	3	0
14	445.5	2.72	2.72	2	91.5	0	1	3	0
15	431.5	3.16	3.16	2	74.43	0	1	2	0
16	449.5	2.11	2.11	2	87.74	4	2	3	0
17	205.2	1.37	1.35	2	66.49	2	4	3	0

Profiles of a CNS drug candidate: [a] Molecular weight: suggested limits, <500 D; preferred range, <450 D. [b] (ACD calculated) Logarithm of octanol/water partition coefficient: suggested limits, 2–5; preferred range, 2–4. [c] Logarithm of the octanol/water distribution coefficient (at a given pH 7.4): suggested limits, 2–5; preferred range, 2–4. [d] Hydrogen bond donors: suggested limits, 0–3; preferred range, 0–1. [e] Polar surface area: suggested limits, <90; preferred range, <70. [f] Suggested limits, 0–8. [g] Extremely low, 0; very low, 1; low, 2; good, 3. [h] Blood-brain barrier: very high penetrant, 0; high, 1; medium, 2; low, 3; undefined, 4. [i] Human intestinal absorption level: good, 0; moderate, 1; poor, 2; very poor, 3.

Table 4. Prediction for the toxicities of compounds **7**–**17**.

Compounds	Rat NTP[a]		Mouse NTP[a]		Ames mutagenicity[b]	DTP[c]
	Male	Female	Male	Female		
7	−3.22	−1.92	−2.29	−3.61	−3.19	−0.947
8	−0.933	−0.0252	−3.1	−1.5	−2.31	−3.08
9	−1.8	−0.175	−2.76	−4.34	−4.08	−1.54
10	2.41	1.11	−0.497	−0.217	9.96	−4.61
11	0.38	−8.28	−3.79	2.01	−9.39	1.13
12	0.38	−8.28	−3.79	2.01	−9.39	1.13
13	0.583	−7.4	−4.83	2.07	−7.66	1.99
14	0.708	−7.34	−4.99	2.29	−8.38	0.319
15	1.5	−8.77	−3.39	2.02	−10.7	0.332
16	−0.523	−11.3	−6.31	2.34	−23.2	−2.11
17	−0.752	−1.13	−1.68	−1.36	0.726	−1.71

[a] U.S. National Toxicology Program: noncarcinogen, NTP <0.3; carcinogen >0.8. [b] Nonmutagen, <0.3; mutagen, >0.8. [c] Developmental toxicity potential: nontoxic, DTP <0.3; toxic, >0.8.

Table 5. Details of LibDockScore, CDOCKER Interaction Energy (kcal/mol), binding energies (kcal/mol), and inhibition constant (Ki) of compounds **7**–**17**.

Compounds	LibDockScore	CDOCKER Interaction Energy	$A_{2A}R$ (PDB code: 3EML)		A_1R (PDB code: 5 N2S)		A_3R (PDB code: 1OEA)	
			Binding Energy	Inhibition Constant	Binding Energy	Inhibition Constant	Binding Energy	Inhibition Constant
7	104.66	−40.15	−8.00	1.36 μM	−7.59	2.75 μM	−6.78	10.69 μM
8	100.80	−36.64	−7.79	1.94 μM	−7.77	2.02 μM	−10.02	45.59 nM
9	107.02	−40.82	−8.05	1.25 μM	−7.42	3.66 μM	−8.83	337.34 nM
10	98.06	−43.66	−7.71	2.21 μM	−7.30	4.48 μM	−7.74	2.11 μM
11	115.27	−42.37	−8.97	268.03 nM	−7.98	1.42 μM	−7.60	2.67 μM
12	113.11	−43.84	−8.92	287.03 nM	−8.14	1.08 μM	−8.05	1.25 μM
13	116.75	−45.85	−9.00	251.78 nM	−9.40	128.28 nM	−6.17	30.09 μM
14	126.00	−45.93	−10.27	29.61 nM	−6.20	28.46 μM	−7.23	5.02 μM
15	117.97	−42.88	−9.57	96.89 nM	−8.15	1.06 μM	−8.54	554.08 nM
16	122.45	−45.29	−7.36	4.04 μM	−7.96	1.46 μM	−7.25	4.81 μM
17	79.32	−31.47	−5.95	43.60 μM	−5.72	64.55 μM	−6.69	12.38 μM
istradefylline	121.74	−51.76	−7.83	1.82 μM	−7.50	3.71 μM	−7.65	2.45 μM

selective or nonselective binding affinities to $A_{2A}R$ of **14** were screened via the same docking procedure. Computational screening results showed that **14** presented higher binding affinity and lower inhibition constant to $A_{2A}R$ than respective to A_1R (PDB code, 5N2S) with −6.20 kcal/mol and 28.46 μM, and A_3R (PDB code, 1OEA) with −7.23 kcal/mol and 5.02 μM (Table 5), which means a preferable selectivity of **14** for binding to $A_{2A}R$.

2.5. Molecular Dynamics Simulations

To demonstrate the reliability of molecular docking results and the stability of **14**-$A_{2A}R$ complex, the RMSD, and the RMSF of **14**-$A_{2A}R$ were investigated via molecular dynamics simulation (Figure 6). The results exhibited that the RMSD of the complex tended to converge to equilibrium during 162 ps, which indicated the system began to reach a stable state. The average

RMSD of the complex was 0.26 nm, which suggested the result of molecular docking is reliable. The RMSF values in the process of molecular dynamics simulation were calculated to study the flexibility of the molecular docking complex. The higher the RMSF value of amino acid is, the more flexible it is in the process of binding. During the whole simulation process, the average RMSF of the complex was only 0.12 nm to the original complex 3EML, suggested that the conformational shift of the complex was small. Statistical residue analysis on non-bond interactions of **14**-A_{2A}R complex (see Table S1 in the Supporting information) showed that top 5 amino acid residues Phe168, Ile274, Leu167, Tyr271, Ile66, and Glu169 presented favorable interactions via hydrophobic and/or hydrogen-bond interactions, and only limited counts exhibited unfavorable interactions (Figures 7A and 7B); top 5 residues Glu169, Phe168, Tyr271, Leu167, and Ile66, as well as top 5 residues Ile274, Leu167, Phe168, Ile66, and Tyr271, displayed hydrogen-bond and hydrophobic interactions, respectively (Figures 7C and 7D).

2.6. Visual Graphic of 14-A_{2A}R Complex Docking

Molecular docking results were analyzed via PyMOL Molecular Graphics System 2.4 and DS20, which presented the sizes and locations of active sites, hydrophobic or hydrophilic, and hydrogen-bond interactions, as well as bonding distances i.e., interaction radius less than 5 Å between the binding sites and the docked compound. Compounds were docked to the active pockets of proteins. Binding poses were observed, and the interactions between ligands and receptors were characterized. The best energetically favorable conformations were chosen from each compound.

The perspective of binding interactions of **14**-A_{2A}R was visualized by PyMOL and DS20 (Figure 8), which showed that the molecule can bind well to the active pocket of A_{2A}R and interact with Phe168 and Glu169 via hydrogen bonds along with the distance of 3.0 Å and 3.7 Å, respectively, with Phe168 via π-π stacked, and form hydrophobic interactions with Leu167, His264, Leu267, Met270, Glu169, Met270, Leu249, Ile274, and Ile66.

3. Conclusions

In summary, seventeen diverse metabolites were discovered from the marine-derived fungus *Aspergillus ochraceus* MCCC 3A00521, including a new benzodiazepine alkaloid (**7**), and a new oxazole derivative (**17**). Compounds **14** and **15**, as prenylated indole alkaloids with piperazine motifs, featured promising potency with their respective EC_{50} values of 2.30 and

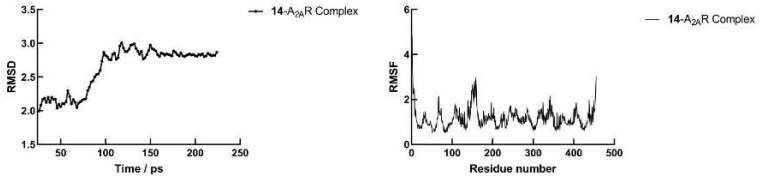

Figure 6. Left: the change of RMSD of backbone atoms in molecular dynamics simulation; Right: the change of RMSF of amino acid residues in molecular dynamics simulation.

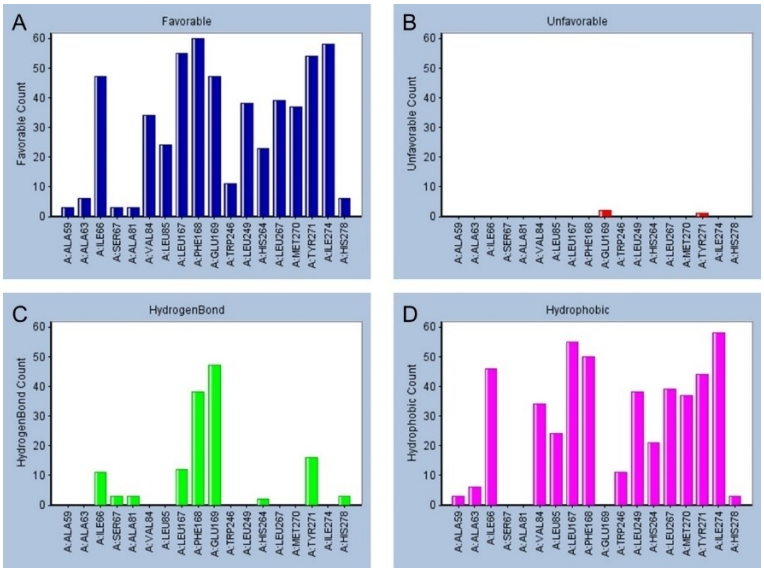

Figure 7. Residue interaction histograms of non-bond interactions of **14**-A_{2A}R complex. A: Residues with favorable interactions; B: Residues with unfavorable interactions; C: Residues with hydrogen bond interactions; D: Residues with hydrophobic interactions.

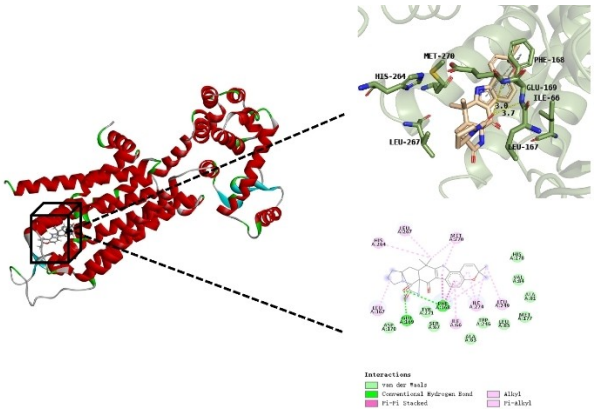

Figure 8. Visual graphic interactions of molecular docking between **14** and $A_{2A}R$. Left: the whole drawing of **14**-$A_{2A}R$; Right: the amplified drawing of **14** docking in pocket sites of $A_{2A}R$ (The above: 3D graphic; The Below: 2D graphic).

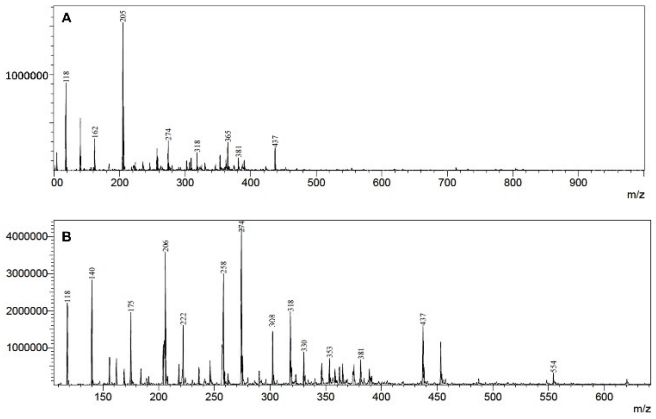

Figure 9. A) MS spectrum of methanol extract of *A. ochraceus* cultivated in PDA-Control; B) MS spectrum of methanol extract of *A. ochraceus* cultivated in PDA-Test.

2.45 μM. Interestingly, compounds **11**–**13** and **16**, which have similar skeletons to those of **14** and **15**, also present lower EC_{50} values towards anti-PD than other types of compounds. ADMET prediction showed **11**–**16** possessed good drug-like characteristics, appropriate features for CNS drugs, and preferable safety scores of toxicities. Extensive virtual screening suggested that these prenylated indole alkaloids with piperazine motifs, **11**–**16**, docking with 3EML, exhibited higher LibDock scores and considerable CDOCKER interaction energies compared to other alkaloids. It is noteworthy that compound **14** not only has better anti-PD activity in vitro, but also exhibited a higher Libdock score than the reference compound istradefylline docking with 3EML. Based on the above analyses, it can be concluded prenylated indole-based compounds with piperazine skeletons have potential anti-PD activity. Amongst them, **13**–**15** with the structure i.e. (epiminomethano)indolizino[6,7-*h*]pyrano [3,2-*a*]carbazole-8,16-dione, exhibited better anti-PD activity. Intriguingly, compound **14**, due to the only structural difference of a carbonyl functional group at C-7, offered both anti-PD activity in vitro and molecular virtual docking screening with better performance than 1**3** and **15**, which provide us an insight into synthesizing its analogies in the next research. ADT programme data have shown that compound **14** possessed a higher binding affinity and a lower inhibition constant to $A_{2A}R$ rather than to A_1R (5N2S) and A_3R (1OEA). Molecular dynamics simulation demonstrated the reliability of molecular docking results and the stability of **14**-$A_{2A}R$ complex in natural environments. These results provided us the first insight into that **14** has the potential as an advantageous lead compound for exploiting highly selective $A_{2A}R$ antagonists for PD therapeutic drugs.

Experimental Section

General Experimental Procedures

TLC was accomplished by silica gel 60 $F_{254+365}$ (Qingdao Ocean Chemical Co., Ltd., China). Silica gel (80–120 and 200–300 mesh; Qingdao Ocean Chemical Co., Ltd., China), RP-C_{18} silica gel (spherical, 20–45 μm, Santai Technologies, Inc., China), and Sephadex LH-20 (Beijing Solarbio Science & Technology Co., Ltd., China) were utilized for column chromatography. HPLC was completed on an Essentia Prep LC-16P with a UV detector via an RP-C18 column (5 μm, 10×250 mm, YMC-Pack, ODS-A). Thermo Fisher LC-LTQ-Orbitrap XL spectrometer was used to collect the HRESIMS data. Bruker AM-400 spectrometer was employed to obtain NMR data as well as taking the solvent peaks (CH_3OH-d_4: δ_H 3.31, δ_C 49.10; DMSO-d_6: δ_H 2.50, δ_C 39.51) as internal references of the ^1H and ^{13}C NMR chemical shifts. JASCO J-810 spectrometer was taken to carry out the ECD spectra measurement. Infrared spectra data were collected via Bruker Vertex 70 equipment. Ultraviolet spectra were analyzed by a Varian Cary 50 instrument. The single-crystal X-ray diffraction data were gathered by a Bruker APEX DUO diffractometer under the graphite-monochromated Cu Kα radiation. The optical rotation measurement was fulfilled by a Perkin-Elmer 341 polarimeter.

Strain Material

The voucher specimens of *Aspergillus ochraceus* MCCC 3A00521 were provided by the Marine Culture Collection of China, which was isolated from the Pacific Ocean. The inoculated strain has been preserved in the Strain Preservation Centre of the School of Life Sciences, Hubei University, China.

Fermentation and Isolation

A. ochraceus MCCC 3A00521 were cultured onto two different PDA culture plates (one only contained PDA, namely PDA-Control; another was added a kind of CYP450 oxidase inhibition 8-geranyloxypsoralen into PDA, namely PDA-Test), then inoculated at 28 °C for a week as seed plates. Two types of methanol extracts of *A. ochraceus* were subjected to LC-MS/MS system to obtain their MS spectra (Figure 9). Since more *m/z* peaks emerged in Figure 9 B, this culture strategy was adopted to amplify the cultivation of *A. ochraceus*. The seed plates were successively hatched into 50 L

conical flasks (100×500 mL, each consisting of the sterilized rice medium) at 25 °C for four weeks for a solid fermentation. The fermented cultures were immersed into 95% ethanol at room temperature for seven days, then a crude extract was obtained after removal of residual ethanol by vacuum distillation. Afterward, the crude extract was sequentially eluted with petroleum ether, chloroform, and ethyl acetate to afford three partitions, respectively. These three portions consecutively underwent column chromatography analyses of silica gel, MPLC (RP-C_{18}, spherical), and Sephadex LH-20. Eventually, semi-preparative HPLC was performed to yield compounds **1**–**6** (from the section of petroleum ether), compounds **7**–**16** (from the section of chloroform), and compound **17** (from the section of ethyl acetate).

Circumdatin N (**7**): Colorless crystals, mp 168–170 °C; $[\alpha]^{20}_{,D}$ +150.9 (*c* 0.35, CH3OH); ECD (MeOH) λ ($\Delta\varepsilon$) 209 (−5.94), 228 (+3.37), 254 (−2.22), and 278 (+0.93) nm; UV (CH3OH) λ_{max} (log ε) = 230 (4.56), 277 (4.06) nm; IR (KBr) ν_{max} = 3375, 3064, 1680, 1661, 1615, 1486, 1469, and 1385 cm^{-1}; ^1H and ^{13}C NMR data, see Table 1; HRESIMS $[M+Na]^+$ *m/z* 330.0839 (calcd for $C_{17}H_{13}N_3NaO_3$, 330.0855).

Ochracesol A (**17**): Colorless crystals, mp 135–137 °C; $[\alpha]^{20}_{,D}$ +35.02 (*c* 0.61, CH_3OH); ECD (MeOH) λ ($\Delta\varepsilon$) 211 (+0.20), 229 (−0.11), 249 (+0.12), 271 (+0.18), and 284 (−0.09) nm; UV (CH_3OH) λ_{max} (log ε) = 274 (4.43), 208 (4.06) nm; IR (KBr) ν_{max} = 3402, 3390, 2938, 1620, 1505, 1446, and 1384 cm^{-1}; ^1H and ^{13}C NMR data, see Table 1; HRESIMS $[M+H]^+$ *m/z* 206.0724 (calcd for $C_{11}H_{12}NO_3$, 206.0817).

Single-Crystal X-Ray Data for Circumdatin N (7)

$C_{17}H_{13}N_3O_3$, M = 307.30, monoclinic, *a* = 26.6757(3) Å, *b* = 4.44940(10) Å, *c* = 12.20820(10) Å, α = 90.00°, β = 98.7560(10)°, γ = 90.00°, *V* = 1432.11(4) $Å^3$, *T* = 100.01(10) K, space group *C*2, *Z* = 4, μ(CuKα) = 0.829 mm^{-1}, 13305 reflections measured, 2840 independent reflections (R_{int} = 0.0255). The final R_1 values were 0.0417 ($I > 2\sigma(I)$). The final $wR(F^2)$ values were 0.1015 ($I > 2\sigma(I)$). The final R_1 values were 0.0419 (all data). The final $wR(F^2)$ values were 0.1017 (all data). The goodness of fit on F^2 was 1.136. Flack parameter = 0.06(6). The Hooft parameter was −0.00(4).

Single-Crystal X-Ray Data for Ochracesol A (17)

$C_{11}H_{11}NO_3$, *M* = 205.21, monoclinic, *a* = 13.14703(11) Å, *b* = 6.88062(4) Å, *c* = 13.19349(11) Å, α = 90.00°, β = 119.0056(11)°, γ = 90.00°, *V* = 1043.782(16) $Å^3$, *T* = 100.01(10) K, space group *P*21, *Z* = 4, μ(CuKα) = 0.798 mm^{-1}, 20222 reflections measured, 4189 independent reflections (R_{int} = 0.0186). The final R_1 values were 0.0305 ($I > 2\sigma(I)$). The final $wR(F^2)$ values were 0.0779 ($I > 2\sigma(I)$). The final R_1 values were 0.0306 (all data). The final $wR(F^2)$ values were 0.0781 (all data). The goodness of fit on F^2 was 1.078. Flack parameter = 0.02(4). The Hooft parameter was 0.01(2).

Deposition Numbers 1961585 (for **17**) and 1961586 (for **7**) contain the supplementary crystallographic data for this paper. These data are provided free of charge by the joint Cambridge Crystallographic Data Centre and Fachinformationszentrum Karlsruhe Access Structures service www.ccdc.cam.ac.uk/structures

Cell Culture and Cytotoxicity Assay

SH-SY5Y cells were incubated in DMEM medium with fetal bovine serum (10%), penicillin G (80 U/mL), and streptomycin (100 U/mL) under a moist atmosphere with 5% CO_2 at 37 °C. Cells were dispensed into a 96-well culture plate with 1×10^4 cells per well. As being grown to 70% confluence, the cells were treated with diluted gradients of all isolates for 24 hours. The medium was discarded before the MTT solution (200 μL, 0.5 mg/mL) was added to each well. After further cultivation for 4 hours, the medium was removed. DMSO (150 μL) was successively added to each well and then shaken to mix it well. The parallel assays were repeated three times. The optical density (OD) of each well was measured via an Envision 2104 multilabel reader (Perkin Elmer, USA). The 50% cytotoxic concentration values (CC_{50}) were calculated using Graphpad Prism 8.

Bioactivities Assay of Compounds on MPP^+ Induced SH-SY5Y Cells SH-SY5Y cells were cultured as the above process. Then cells in the logarithmic growth phase were inoculated into a 96-well plate (1×10^4 cells/well) with 6 multiple wells in each group. The assay was set up three groups: normal control group, being added 200 μL DMEM medium; model group, being added 200 μL DMEM medium containing MPP^+ with the concentration 1 mM;[25] drug group, one hour before added MPP^+, being added designated concentrations of compounds or the positive control. All groups were cultivated for 24 hours. The following operations were performed similarly to the above-mentioned. The 50% effective concentration values (EC_{50}) were simulated via Graphpad Prism 8.

Virtual Screening Details

Structures of isolated alkaloids were established by ChemOffice 2018 program, and the geometries energies were optimized via Gaussian 16 at the B3LYP/6-311G(d,p) level. PDB crystal structures were downloaded from RCSB PDB database and PDB site records were selected as the binding sites to screen the prepared alkaloids for selected $A_{2A}R$ antagonists. Virtual screening was implemented via the LibDock programme of DS20. The minimization algorithm was performed using Smart Minimizer at CHARMm Minimization Forcefield level. All binding poses of compounds were sorted based on the LibDockScore.

CDOCKER module of DS20 is a high precision procedure, which is based on CHARMm force field, and regarded proteins as rigid and ligands as flexible for molecular docking. PDB crystal structures were imported and prepared via DS20 tools. The previously treated alkaloids were used to process docking. the binding site spheres were defined according to PDB site records. Finally, a plurality of different conformations of each ligand-protein complex was obtained, which were further analyzed based upon CDOKER interaction energies.

The created .mol2 files of prepared alkaloids by Gaussian 16 were saved as .pdb via PyMOL 2.4. 3D coordinates of A_1R (PDB code, 5N2S), $A_{2A}R$ (PDB code, 3EML), and A_3R (PDB code, 1OEA) were downloaded as .pdb format from RCSB protein database. Autodock demands ligands and receptor portrayals in .pdbqt format files, which belong to the modified protein data bank[31] format involving atom type definitions, atomic charges, and topological information (rotatable bonds) for ligands. The .pdb molecules were submitted to Autodock Tool 4.2 (ADT) to generate .pdbqt files after being checked charges and detected torsion numbers. Being removed water molecules and redundant atoms, the macromolecules (receptors) were added hydrogens, Gasteiger charges, and were assigned AD4 atom types to create .pdbqt files.[32] AutoGrid was utilized to generate grid maps. The grid boxes were established according to the active pockets of the original protein crystal structures. Docking works were performed with the default parameters under the Lamarckian Genetic Algorithm. Positional Root Means Quare Deviation (RMSD) tolerance of 2.0 Å was considered optimal and clustered together for the advantageous binding search.

Molecular Dynamics Simulation Details

According to the docking results of CDOCKER, the **14**-A_{2A}R complex with the best pose was selected and processed for molecular dynamics simulation. The simulation was carried out with the natural pressure as well as nearly 300 K temperature during the whole experiment. The CHARMm force field was applied, then the complex solvation was subjected in an orthorhombic cell shape and an explicit periodic boundary model. The standard dynamics cascade method was performed to run molecular dynamics simulation of **14**-A_{2A}R complex. The equilibration time lasted for 20 ps. The simulation of production was operated for 200 ps with a time step of 2 fs. Taken original A_{2A}R as a reference, the trajectory of **14**-A_{2A}R complex was analyzed for RMSD to conformations and RMSF of amino acid residues.

Statistical Analysis

Data of the experiments were shown as means ± SD and analyzed via the Student's t-test or one-way ANOVA. Statistic data were achieved by using GraphPad Prism 8.0. The value of $P < 0.05$ was of statistical significance.

Acknowledgements

This work was financially supported by the National Natural Science Foundation of China (Nos. 31700298 and 31700294), National & Local Joint Engineering Research Center of High-throughput Drug Screening Technology (Hubei Province, China) (M20181008), Innovation and Entrepreneurship Training Program for Undergraduates (Hubei Province, China) (Nos. S201910512010 and S202010512054), and Pharmaceutical "Jingchu Outstanding Talent" Collaborative Education Program and Innovative Training Program for Undergraduates (Hubei University, China) (M20191003). We expressed our sincere thanks to Dr. Xin Zhou (Institute of Materia Medica, Chinese Academy of Medical Sciences & Peking Union Medical College) for the SH-SY5Y cell line.

Conflict of Interest

The authors declare no conflict of interest.

Keywords: adenosine receptors · *Aspergillus ochraceus* · alkaloids · drug discovery · Parkinson's disease · virtual screening

[1] C. A. Davie, *Br. Med. Bull.* **2008**, *86*, 109–127.
[2] T. J. Moore, J. Glenmullen, D. R. Mattison, *Jama* **2014**, *174*, 1930–1933.
[3] W. K. D. Ko, S. M. Camus, Q. Li, J. Yang, S. McGuire, E. Y. Pioli, E. Bezard, *Neuropharmacology* **2016**, *110*, 48–58.
[4] I. Delgadillo, *Mycotoxin Res.* **1986**, *2*, 9–17.
[5] Y. Tan, B. Yang, X. Lin, X. Luo, X. Pang, L. Tang, Y. Liu, X. Li, X. Zhou, *J. Nat. Prod.* **2018**, *81*, 92–97.
[6] Y. Fan, Y. Zhou, Y. Du, Y. Wang, P. Fu, W. Zhu, *Mar. Drugs* **2019**, *17*.
[7] J. Fuchser, A. Zeeck *Liebigs Ann.* **1997**, *1*, 87–95.
[8] C. M. Cui, X. M. Li, M. Li, C. S. Li, C. G. Huang, B. G. Wang, *J. Nat. Prod.* **2010**, *73*, 1780–1784.
[9] a) F. D. Guzman, J. B. Gloer, D. T. Wicklow, P. F. Dowd, *J. Nat. Prod.* **1992**, *55*, 931–939; b) L. Rahbæk, J. Breinholt, *J. Nat. Prod.* **1999**, *62*, 904–905; c) J. R. Dai, B. K. Carté, P. J. Sidebottom, A. L. S. Yew, S. B. Ng, Y. Huang, M. S. Butler, *J. Nat. Prod.* **2001**, *64*, 125–126; d) Y. W. Chang, C. M. Yuan, J. Zhang, S. Liu, P. Cao, H.-M. Hua, Y. T. Di, X. J. Hao, *Tetrahedron Lett.* **2016**, *57*, 4952–4955; e) H. Wen, X. Liu, Q. Zhang, Y. Deng, Y. Zang, J. Wang, J. Liu, Q. Zhou, L. Hu, H. Zhu, C. Chen, Y. Zhang, *Chem. Biodiversity* **2018**, *15*, e1700550; f) Y. Fan, Y. Zhou, Y. Du, Y. Wang, P. Fu, W. Zhu, *Mar. Drugs* **2019**, *17*; g) L. Rahbaek, J. Breinholt, J. C. Frisvad, C. Christophersen, *J. Org. Chem.* **1999**, *64*, 1689–1692; h) F. Wang, Z. Hu, C. Li, X. Wu, S. Cao, *Tetrahedron Lett.* **2019**, *60*, 1724–1726.
[10] M. Balcells, R. Canela, J. Coll, V. Sanchís, M. Torres, *J. Pestic. Sci.* **1995**, *45*, 319–323.
[11] J. Wang, W. He, F. Kong, X. Tian, P. Wang, X. Zhou, Y. Liu, *J. Nat. Prod.* **2017**, *80*, 1725–1733.
[12] C. Zhang, L. Hu, D. Liu, J. Huang, W. Lin, *Front. Pharmacol.* **2020**, *11*, 760.
[13] E. H. Driche, S. Belghit, C. Bijani, A. Zitouni, N. Sabaou, F. Mathieu, B. Badji, *Ann. Microbiol.* **2014**, *65*, 1341–1350.
[14] D. N. Quang, D. D. Bach, *Nat. Prod. Res.* **2008**, *22*, 901–906.
[15] T. Amagata, M. Tanaka, T. Yamada, M. Doi, K. Minoura, H. Ohishi, T. Yamori, A. Numata, *J. Nat. Prod.* **2007**, *70*, 1731–1740.
[16] X. H. Liu, F. P. Miao, X. R. Liang, N. Y. Ji, *Nat. Prod. Res.* **2014**, *28*, 1182–1186.
[17] Z. B. Tong, X. H. Cui, J. Wang, C. L. Zhang, Y. Y. Zhang, Z. J. Ren, *Nat. Prod. Res.* **2017**, *31*, 2564–2567.
[18] T. A. Mansoor, J. Hong, C. O. Lee, S. J. Bae, K. S. Im, J. H. Jung, *J. Nat. Prod.* **2005**, *68*, 331–336.
[19] J. Peng, X. Y. Zhang, Z. C. Tu, X. Y. Xu, S. H. Qi, *J. Nat. Prod.* **2013**, *76*, 983–987.
[20] J. B. Bremner, W. Sengpracha, I. Southwell, C. Bourke, B. W. Skelton, A. H. White, *Aust. J. Chem.* **2004**, *57*, 273–276.
[21] H. Kato, T. Yoshida, T. Tokue, Y. Nojiri, H. Hirota, T. Ohta, R. M. Williams, S. Tsukamoto, *Angew. Chem. Int. Ed. Engl.* **2007**, *46*, 2254–2256.
[22] K. A. Miller, S. Tsukamoto, R. M. Williams, *Nat. Chem.* **2009**, *1*, 63–68.
[23] S. S. Afiyatullov, O. I. Zhuravleva, A. S. Antonov, D. V. Berdyshev, M. V. Pivkin, V. A. Denisenko, R. S. Popov, A. V. Gerasimenko, G. von Amsberg, S. A. Dyshlovoy, E. V. Leshchenko, A. N. Yurchenko, *J. Antibiot.* **2018**, *71*, 846–853.
[24] S. Tsukamoto, H. Kato, M. Samizo, Y. Nojiri, H. Onuki, H. Hirota, T. Ohta, *J. Nat. Prod.* **2008**, *71*, 2064–2067.
[25] C. Kim, S. Park, *Endocr. Connect.* **2018**, *7*, 443–455.
[26] H. Xie, M. Chang, X. Hu, D. Wang, M. Tian, G. Li, H. Jiang, Y. Wang, Z. Dong, Y. Zhang, L. Hu, *Neurol. Sci.* **2011**, *32*, 221–228.
[27] A. Lipinski Christopher, *Drug Discovery Today Technol.* **2004**, *1*, 337–341.
[28] A. M. Palmer, M. S. Alavijeh, *Drug Discovery Today* **2012**, *17*, 1068–1078.
[29] M. Ruiz, Y. H. Lim, J. Zheng, *J. Med. Chem.* **2014**, *57*, 3623–3650.
[30] Umesh, D. Kundu, C. Selvaraj, S. K. Singh, V. K. Dubey, *J. Biomol. Struct. Dyn.* **2021**, *39*, 3428–3434. DOI: 10.1080/07391102.2020.1763202 .
[31] H. M. Berman, J. Westbrook, Z. Feng, G. Gilliland, T. N. Bhat, H. Weissig, I. N. Shindyalov, P. E. Bourne, *Nucleic Acids Res.* **2000**, *28*, 235–242.
[32] M. K. Parvez, M. Tabish Rehman, P. Alam, M. S. Al-Dosari, S. I. Alqasoumi, M. F. Alajmi, *Saudi Pharm. J.* **2019**, *27*, 389–400.

Manuscript received: January 25, 2021
Revised manuscript received: April 17, 2021